RAA 2015 Vol. **15** No. **7**, 1057–1067 doi: 10.1088/1674–4527/15/7/013
http://www.raa-journal.org *http://www.iop.org/journals/raa*

*R*esearch in
*A*stronomy and
*A*strophysics

Terrain reconstruction from Chang'e-3 PCAM images *

Wen-Rui Wang, Xin Ren, Fen-Fei Wang, Jian-Jun Liu and Chun-Lai Li
National Astronomical Observatories, Chinese Academy of Sciences, Beijing 100012, China;
renx@nao.cas.cn

Received 2014 July 22; accepted 2014 December 10

Abstract The existing terrain models that describe the local lunar surface have limited resolution and accuracy, which can hardly meet the needs of rover navigation, positioning and geological analysis. China launched the lunar probe Chang'e-3 in December, 2013. Chang'e-3 encompassed a lander and a lunar rover called "Yutu" (Jade Rabbit). A set of panoramic cameras were installed on the rover mast. After acquiring panoramic images of four sites that were explored, the terrain models of the local lunar surface with resolution of 0.02 m were reconstructed. Compared with other data sources, the models derived from Chang'e-3 data were clear and accurate enough that they could be used to plan the route of Yutu.

Key words: space vehicles: rover — space vehicles: instruments: panoramic camera — methods: terrain reconstruction — techniques: image processing: orthoimage

1 INTRODUCTION

Three-dimensional (3D) terrain reconstruction is a direct way to model the surface characteristics of a planetary body. There have been a number of lunar probes orbiting the Moon. Among these, Clementine (Smith et al. 1997), SELenological and Engineering Explorer (SELENE) (Araki et al. 2009), Lunar Reconnaissance Orbiter (LRO) (Smith et al. 2010) and Chang'e-1 (Li et al. 2010) obtained global maps of the Moon with different resolutions and accuracies. However, none of them could resolve fine local terrain texture. In addition, 20 soft landers from the Luna and Apollo series carried cameras, but they did not provide integrated coverage of their landing area that Chang'e-3 was able to acquire. Thus reconstructing a high resolution and highly accuracy terrain model is one of the primary objectives of Chang'e-3. The Chang'e-3 mission was composed of a soft lander and a rover called Yutu. The lander carried four scientific payloads including a terrain camera (TCAM), a descending camera, a lunar-based ultraviolet telescope (LUT) and an extreme ultraviolet (EUV) camera, while the rover was equipped with a panoramic camera (PCAM), Ground Penetrating Radar (GPR), the VIS/NIR Imaging Spectrometer (VNIS), and the Alpha Particle X-Ray Spectrometer (APXS). Located on the top mast of Yutu, the PCAM acquired 3D imagery of the lunar surface for surveying the terrain, geological features and structures, and craters inside the target region. It also monitored the operational state of the lander. The PCAM had both panchromatic and color working modes, and it photographed the lander in static color mode at six separate sites after they were separated. During the first two working periods, Yutu maneuvered around the lander, photographed it at six sites and obtained panoramic images of the topography at four sites. During the process of acquiring panoramic images, the pitch angles (the angle from the horizontal axis to the optical axis) of PCAM were –7° and –19°, while the yaw angle (the rotation angle around the mast) was –13°.

∗ Supported by the National Natural Science Foundation of China.

2 IMAGING MODE

As a set of binocular stereo vision instruments, the PCAM on the rover mast is composed of two cameras with similar constructions, and the distance between their principal centers is called the baseline. Both cameras that are part of PCAM capture 2D images of a certain scene simultaneously, construct a stereo image pair and match the identical points. With the 3D coordinates of those matching points, depth or distance to a target can be reconstructed. The focal length of Chang'e-3's PCAM is about 50 mm with a field of view (FOV) of 19.7° × 14.5°. A Charge-Coupled Device (CCD) with dimensions 2352 × 1728 is used for color imaging mode, and for panchromatic mode the dimensions are 1176 × 864. The pixel size of the CCD is 7.4 µm (Tan et al. 2014). The two cameras are separated by a 27 cm baseline, and the angle between the principal axis and baseline is 1°. This angle ensures there is enough parallax in the image pair as shown Table 1.

Table 1 Technical Indexes of PCAM

No	Character	Value
1	Waveband	Visible light
2	Color	(R, G, B)
3	Imaging mode	Color mode/Panchromatic mode (switchable)
4	Imaging distance (m)	$3\sim\infty$
5	Frame size	2352 × 1728 (color), 1176 × 864 (panchromatic)
6	CCD Pixel size	7.4 µm
7	FOV (°)	19.7° × 14.5°
8	Quantized value (bit)	10
9	S/N (dB)	≥40 (maximum) ≥30 (albedo: 0.09, solar elevation: 30°)
10	MTF	≥0.20 (full FOV)
11	Compressed or not	uncompressed

The rover mast on Yutu has two degrees of freedom, meaning that the PCAM can rotate from –180° to +180° horizontally and from –90° to +90° vertically. The PCAM elevation above the lunar surface is about 1.596 m. As the slope of the local topography has been taken as 0°, the range of visibility was totally determined by the camera specifications. The triangular geometry shows that the horizontal visibility range reaches as far as 2379.2 m. For the minimum visibility range, the calculation uses Equation (1)

$$\mathrm{S_{min}} = \frac{h}{\tan(\theta + \phi/2)}\,, \tag{1}$$

where $\mathrm{S_{min}}$ is the minimum visibility range, h is the elevation of PCAM above the lunar surface, θ is the pitch angle, and ϕ is the vertical FOV. For the maximum visibility range, the calculation uses Equation (2)

$$\mathrm{S_{max}} = R\ \arccos(R/(R+h))\,, \tag{2}$$

where $\mathrm{S_{max}}$ is the maximum visibility range and R is the mean radius of the Moon.

In Table 2, the pitch angles, and the nearest and farthest visibility ranges corresponding to each pitch angle are listed in the columns.

As the rover has a square base, when the pitch angle of PCAM is lower than –31°, the base of the rover will unavoidably appear in some images, and reduce the amount of information about the topography. For this reason, most of the images taken during the third lap contribute little to the process of terrain reconstruction. The PCAM on Yutu adjusted pitch twice (–7° and –19°) at each exploration site to achieve the best coverage and efficiency. Close-range photogrammetry using PCAM on Yutu has its own special characteristics. The resolution and accuracy differ according to the imaging range. The farther the range is, the larger the coverage will be, and resolution and

Table 2 Pitch Angles and Visibility Ranges

Pitch Angle (°)	0°–12°–24°		1°–13°–25°		2°–14°–26°		3°–15°–27°	
Number of turns	2 laps	3 laps	2 laps	3 laps	2 laps	3 laps	2 laps	3 laps
Nearest (m)	5.1	3.1	4.8	3.0	4.6	3.0	4.4	2.9
Farthest (m)	2379.2	2379.2	2379.2	2379.2	2379.2	2379.2	2379.2	2379.2
Pitch Angle (°)	4°–16°– 28°		5°–17°– 29°		6°–18°– 30°		7°–19°– 31°	
Number of turns	2 laps	3 laps	2 laps	3 laps	2 laps	3 laps	2 laps	3 laps
Nearest (m)	4.3	2.8	4.1	2.7	4.3	2.8	4.1	2.7
Farthest (m)	2379.2	2379.2	2379.2	2379.2	2379.2	2379.2	2379.2	2379.2

accuracy will be reduced accordingly. When the Yutu rover is moving, scientists need updated local terrain models in real time to guide their decisions. So, the maximum range for the reconstructed models is 50 m.

3 TOPOGRAPHY AND IMAGE CHARACTERISTICS

Chang'e-3 soft-landed on 2013 December 14 at 13:11 UTC. The landing site (44.12° N, 19.50° W) (Huang et al. 2014) was located in Mare Imbrium, about 40 km south of Laplace F. After departure from the Lander, the Yutu rover started its working period that lasted three months. During the first two months, Yutu imaged the topography at exploration sites N0106, N0108, N0203 and N0205 (Fig. 1). Thanks to the overlaps between neighboring site images, we can connect the four site models into a strip, convenient for integrated route planning.

Figure 1 shows the planned route for the Yutu rover, in which the red circles are navigation sites and the blue stars are exploration sites.

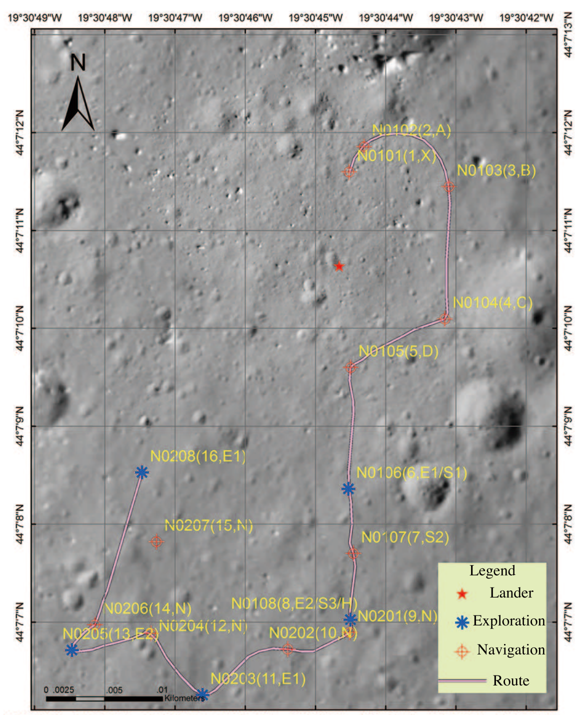

Fig. 1 Sketch of the route taken by the rover.

4 METHOD FOR SINGLE SITE RECONSTRUCTION

As the texture of lunar images is neither rich nor distinct, and the grey levels change with lighting, it is not easy to implement the reconstruction method used by other planet rovers because of the specific PCAM and lunar images, so a process suitable for Chang'e-3 has to be developed (Fig. 2).

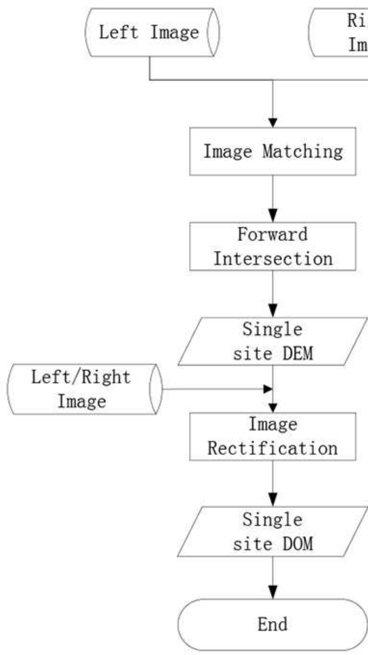

Fig. 2 Real-time processing of Chang'e-3 PCAM 3D terrain models.

The 3D reconstruction contains the following steps: the raw image pairs are preprocessed and those images after dark current correction, radiometric correction, photometric calibration, geometry correction and color restoration, if they represent the lunar surface well, are considered to be qualified input images. With the exterior orientation parameters, the positions and attitudes of image pairs are determined, and identical points on the left and the right image are matched by applying scale invariant feature transform (SIFT) and Harris operators, which are feature matching methods. The 3D coordinates of identical points are calculated using forward intersection, and a triangulated irregular network (TIN) can be constructed with the scatter points. The TIN forms the skeleton of the Digital Elevation Model (DEM), and a Digital Orthophoto Map (DOM) is generated after digital differential rectification. Considering the need for positioning and navigation, as well as processing speed, we select 0.02 m as the resolution of DEM and DOM. For the data preprocessing, radiometric calibration, geometric positioning and color restoration are needed. Also, the interior and exterior orientation parameters are necessary inputs for the following procedure. Usually, the interior orientations are obtained from the ground calibration experiment (Wu et al. 2013). The parameters include focal lengths, principal point offset and lens distortions. In order to reach a high precision, the target should be set in different positions, and at least 50% of the image FOV should be occupied by the target. Calculations of exterior orientation parameters are based on the rover attitude and position in the coordinate system used in this work, its pitch angle, yaw angle and roll angle, installation parameters of PCAM, and the relative orientation between the left and right cameras. The position and attitude of the rover and the attitudes of the mast are obtained from the real time telemetry data, and the installation parameters of the cameras are from the ground calibration. From the above parameters, the exterior orientation parameters are estimated. SIFT operator is an extreme value based method, which has the goal of finding local image features. It remains stable, informative and extensible when changes in rotation, scale or illumination are applied. Harris operator is able to ensure uniformity, reasonability and stability of image corner extraction (Tang et al. 2013). Combining SIFT operator and Harris operator together does not employ new calculations and reduces the relative complexity of the algorithm. The introduction of least squares matching and epipolar constraints converts the two-dimensional search to a one-dimensional search and further improves matching efficiency. With such a matching technique, an average of about 1000 points was extracted from each PCAM image pair. The minimum matching error was 0 pixels, the maximum error was 1.2 pixels, and the standard deviation was 0.3 pixels. Figure 3 shows a pair of Yutu PCAM images and the distribution of identical points. These points fully cover the range in the image, and we can hardly find any errors in the computed locations of points.

After applying forward intersection of dense identical points, their 3D coordinates were obtained. We can reconstruct the single site DEM by filtering and interpolating cloud points. We chose TIN as the interpolation method, which has a resolution of 0.02 m. The TIN is a digital data structure for the representation of a surface. It is often derived from the elevation data of a rasterized DEM. An advantage of using a TIN over a raster DEM in mapping and analysis is that the points computed with a TIN are variably distributed based on an algorithm that determines which points are most necessary for an accurate representation of the terrain. Data input is therefore flexible and fewer points need to be stored than in a raster DEM with regularly distributed points. The DOM for a single site was drawn from left or right image rectification. Image rectification methods can be classified into optical-mechanical rectification, optical differential rectification and digital differential rectification. Digital differential rectification uses the orientation parameters, exterior orientation elements and DEM, with a certain mathematical model to calculate orthoimages from non-orthographic ones. This process will divide the image into many small regions, and rectify them one by one (Rainer 1980). Digital differential rectification can overcome the limitation of optical rectification, and it was applied in this paper.

5 TERRAIN MODEL AND PRELIMINARY ANALYSIS

5.1 Terrain Models of Exploration Sites

With the PCAM images obtained during the first two months, 0.02 m DEM and DOM of four exploration sites were reconstructed. Figure 4 shows the results of sites N0106 and N0108. The left panels are DEM and the right panels are DOM.

As mentioned by Li et al. (2014), the topography of a region with area 4 km $\times$ 4 km near the landing site is flat, with an average elevation of –2639 m. The overall terrain shows an inclining trend from west to east. The exploration sites N0106 and N0108 were detected in the first lunar day, and they are located toward the south of the landing site. In DEMs of Figure 4, boundaries running from northwest to southeast can be obviously seen, dividing the topography into a western higher part and an eastern lower part. As the overall terrain of the landing area is flat, there are few large craters. In both sites, the largest craters we can see are smaller than 10 meters, and their diameters and depth show young geologic ages.

5.2 Accuracy Assessment

According to the reconstruction method, the DEM errors are mainly caused by the following factors: (1) deformation of the raw image; (2) interior orientation error; (3) exterior orientation error; (4) matching error; (5) interpolation error. For DOM, the image rectification error should be taken into consideration. As is well known, a precision analysis of the terrain model includes the inner and

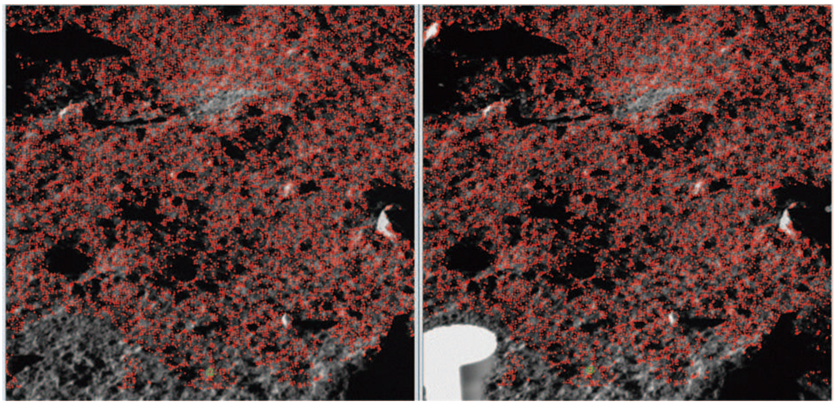

Fig. 3 Distribution of identical points in the PCAM image pair.

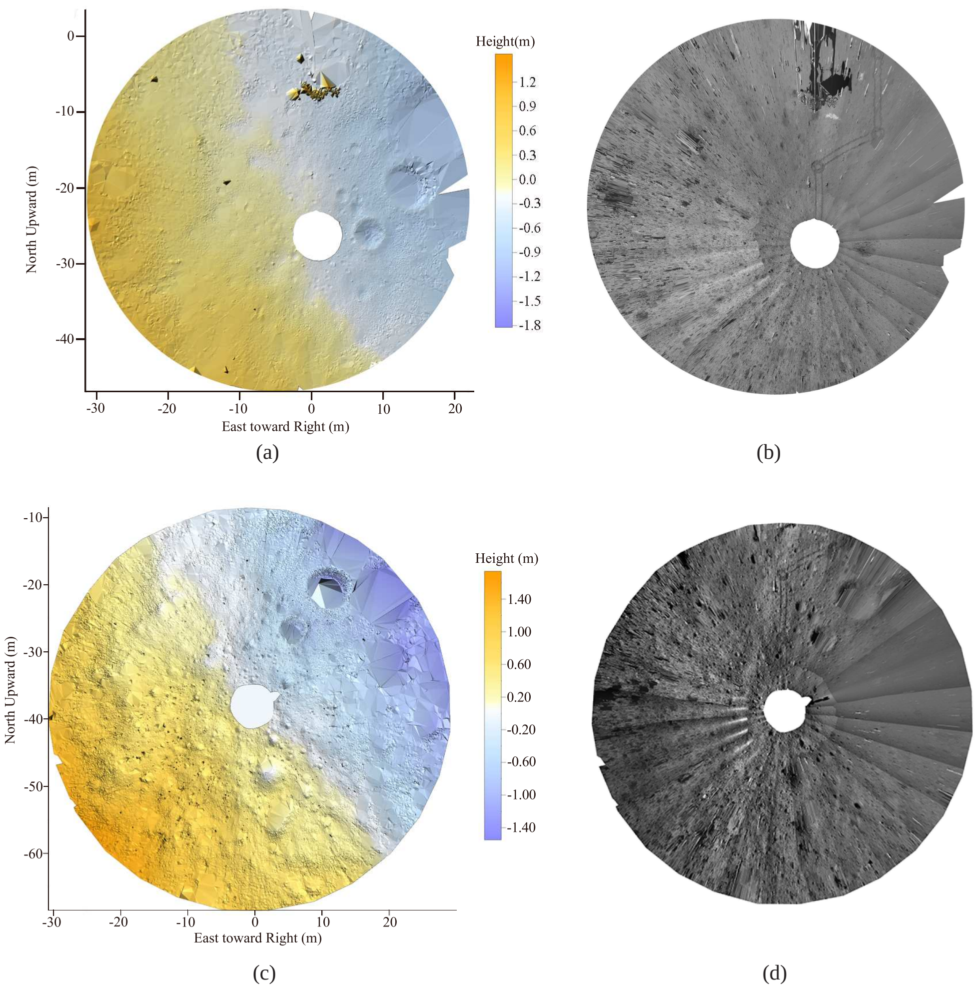

Fig. 4 DEM and DOM of sites N0106 (*top*) and N0108 (*bottom*). The left panels are DEM and the right panels are DOM, with a resolution of 0.02 m.

the outer precision analysis, which is described in subsections 5.2.2–5.2.4. The inner precision of our terrain models can be evaluated by the relationship between adjacent images while the outer precision can be evaluated by comparing with other terrain data. Although the five lunar absolute control points provide good references, the long distance between the Chang'e-3 landing site and the five control points will cause errors to accumulate and make the comparison inaccurate. For this reason, we evaluate the inner and the outer precisions by following the steps below.

5.2.1 Inner precision analysis

The overlaps between adjacent images can be used to connect the exploration sites into a strip along the rover route. We select a set of uniformly distributed identical points in the overlapping area, measure their coordinates and make comparison. Take site N0106 for example, among the 24 identical points, the maximum deviation along the East direction is –0.023 m, and the maximum deviation along the North direction is –0.028 m. They are less than 2 pixels, which is hard for the eyes to distinguish. This shows that without adjustment, the adjacent images connect with each other smoothly, so the reconstructed terrain models have high inner precision.

5.2.2 Outer precision analysis: compared with descending image

During the descent of Chang'e-3, the descending camera captured an image series that had differing resolutions. These images with views of the landing area were resampled and georeferenced on the basemap composed of Chang'e-1 images of the entire Moon that have a resolution of 120 m and then compared with the PCAM terrain models (Fig. 5). The corresponding craters near the Yutu rover both in the descending image and in the PCAM DOM were marked, and the range from the center of the rover to the center of the crater was measured. The results are shown in Table 3.

In Table 3, the maximum difference in distance is 0.73 m, and the minimum difference is 0.19 m. The maximum difference relative to distance is about 4.5%.

5.2.3 Outer precision analysis: compared with telemetry data

In Figure 6, five navigation points (N0201, N0106, N0105, N0104, N0103) can be easily recognized by following the rover tracks, and the distances between neighboring points are listed in Table 4.

In Table 4, the differences between DOM distance and the distance as computed by telemetry fall below 1 m, and the differences may come from errors in the rover position as computed from telemetry and in exterior orientation.

Table 3 Statistics Describing Distance in the Descending Images and PCAM DOM

Crater ID	Distance in descending image (m)	Distance in PCAM DOM (m)	Distance difference (m)	Percentage of the difference to descending image distance (%)	Percentage of the difference to PCAM distance (%)
C1	16.97	16.24	0.73	4.30	4.50
C2	15.67	15.21	0.46	2.94	3.02
C3	13.15	12.80	0.35	2.66	2.73
C4	21.27	20.55	0.72	3.39	3.50
C5	6.17	6.36	–0.19	3.08	2.99
C6	10.50	10.27	0.23	2.19	2.24
C7	16.96	17.63	–0.67	3.95	3.80

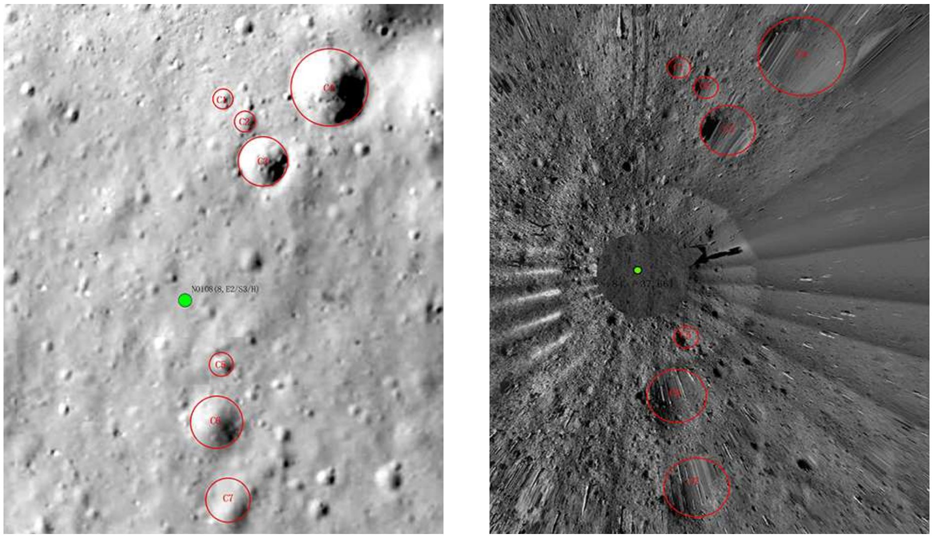

(a) (b)

Fig. 5 Craters are denoted with red circles in the descending image (a) and PCAM DOM "Descending image" (b).

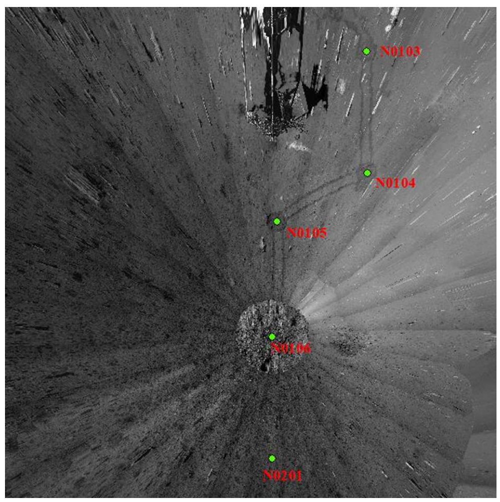

Fig. 6 Five navigation points.

5.2.4 Outer precision analysis: compared with an image taken by LRO

On 2013 December 30, NASA published images of the Chang'e-3 lander and rover that were taken by the narrow angle camera that is part of LRO. At the time images were acquired, Yutu was located at site S3. Two arrows indicate the locations of both the lander and the rover (Fig. 7), and their distance can be calculated with the scale used by the image. The image taken by LRO helps to test both the landing accuracy of Chang'e-3, and also the accuracy of our reconstructed model. In

Table 4 Statistics Describing Telemetry Distance and Distance in PCAM DOM

	PCAM DOM distance (m)	Telemetry distance (m)	Distance difference (m)	Percentage of the difference to PCAM distance (%)	Percentage of the difference to telemetry distance (%)
N0201–N0106	11.0	12.0	1.0	9.09	8.33
N0106–N0105	10.34	10.04	–0.3	2.90	2.99
N0105–N0104	9.23	9.75	0.52	5.63	5.33
N0104–N0103	10.95	11.16	0.21	1.92	1.88

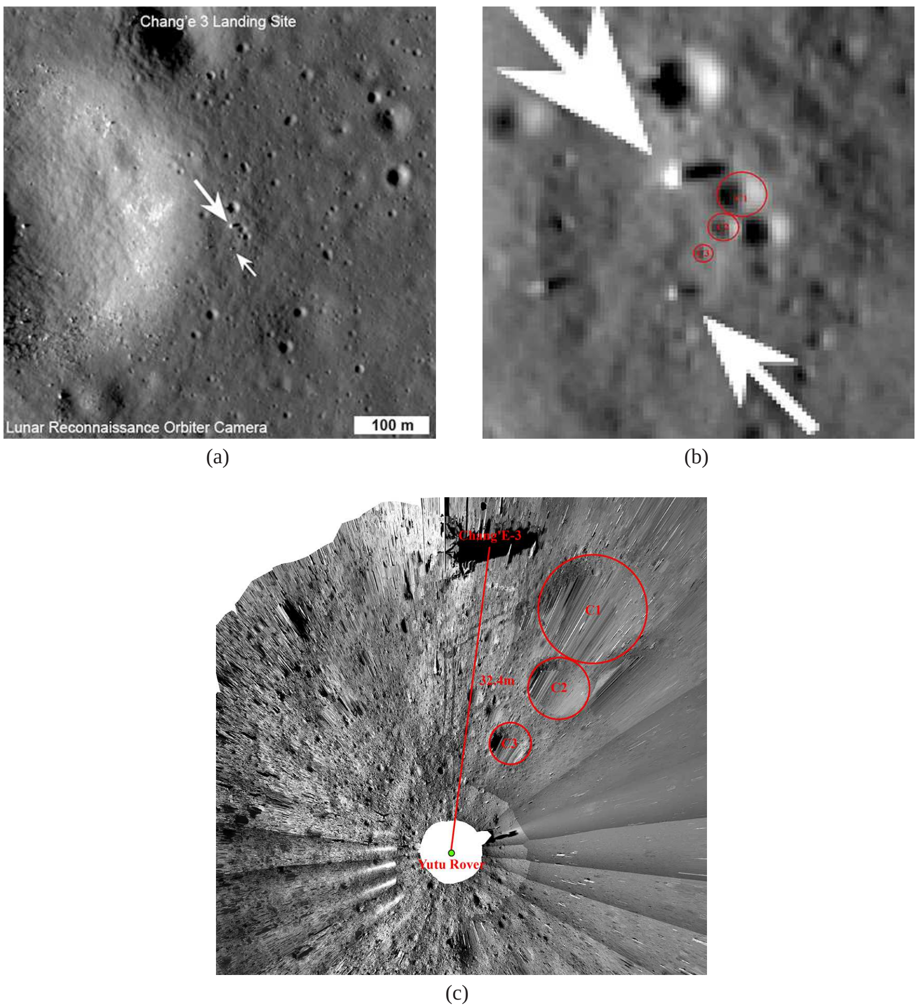

Fig. 7 LRO NAC image (Robinson et al. 2014) and PCAM DOM of site S3. (a) The LRO NAC image, where the larger arrow indicates the location of the lander, and the smaller arrow indicates the position of the rover. (b) The enlarged part of three identified craters. (c) PCAM DOM of site S3, with the same craters marked.

the LRO image, 32 pixels represent 32 m, and in the PCAM DOM, the measured distance is about 32.4 m. The relative difference is 0.4 m, 1.3% at a range of 30 m. This validates the data processing method used in the reconstruction, and demonstrates the positioning accuracy of DOM.

We can easily recognize three craters in both the LRO image and in the PCAM DOM. These craters are marked with red circles. We measured the distances between the rover and crater centers, and the results are listed in Table 5.

Table 5 Statistics Describing Distance in the LRO Image and PCAM DOM

Crater ID	Distance in LRO image (m)	Distance in PCAM DOM (m)	Distance difference (m)	Percentage of the difference to LRO image distance (%)	Percentage of the difference to PCAM distance (%)
C1	30.2	30.3	0.1	0.3	0.3
C2	22.0	21.2	0.8	3.6	3.8
C3	13.6	13.2	0.4	2.9	3.0

Similar to the comparisons between descending image and PCAM DOM, the maximum difference in distance is 0.8 m, and the minimum difference is 0.1 m. The maximum difference relative to distance is about 3.8%. Considering that the descending image and the LRO image are perfectly calibrated and georeferenced, they can be used as a standard to evaluate the relative accuracy of PCAM DOM. From the above comparisons, we find that the reconstructed DOMs accurately reproduce the crater shape, as well as the spatial distances. The horizontal accuracy of PCAM DOM is high enough for surveying the terrain and planning a route for the rover.

6 CONCLUSIONS AND DISCUSSION

Through analyzing the imaging mode of PCAM mounted on Chang'e-3 and characteristics of the associated close-range photogrammetry, and considering the need for rover route planning while working efficiently, we chose 0.02 m as the average resolution, and generated the DEM and DOM of four exploration sites during the first two months. Their precisions are evaluated in several aspects. By comparing the relationship between adjacent images and adjacent sites, the accuracy between adjacent DOMs is less than two pixels (in the PCAM DOM with a 0.02 m resolution, two pixels is equal to 0.04 m), which is hard for the eyes to distinguish. The outer precision analysis mainly comes from the distance measurement. The differences in distance between DOM and descending image, DOM and telemetry data, and DOM and LRO image are so small that the largest relative error did not exceed 10%. Although the five lunar absolute control points whose coordinates have been determined by the lunar laser ranging provide good references for precision analysis, the long distance between the Chang'e-3 landing site and the five control points will cause errors to accumulate and make the comparison inaccurate. With the development of a lunar control network, it is possible that the terrain models in future missions will have absolute control points for validating accuracy.

Acknowledgements This work was funded by the National Natural Science Foundation of China (Grant Nos. 41371414 and 41304021).

References

Araki, H., Tazawa, S., Noda, H., et al. 2009, Science, 323, 897
Huang, Y., Chang, S., Li, P., et al. 2014, Chinese Science Bulletin, 59, 3858
Li, C., Liu, J., Ren, X., et al. 2010, Science China Earth Sciences, 53, 1091
Li, C.-L., Mu, L.-L., Zou, X.-D., et al. 2014, RAA (Research in Astronomy and Astrophysics), 14, 1514

Rainer, H. 1980, in Congree of the International Society for Photogrammetry, 294
Robinson, M. S., Plescia, J. B., & Wagner, R. V. 2014, in Lunar and Planetary Science Conference, 45, 1859
Smith, D. E., Zuber, M. T., Neumann, G. A., & Lemoine, F. G. 1997, J. Geophys. Res., 102, 1591
Smith, D. E., Zuber, M. T., Jackson, G. B., et al. 2010, Space Sci. Rev., 150, 209
Tan, X., Liu, J.-J., Li, C.-L., et al. 2014, RAA (Research in Astronomy and Astrophysics), 14, 1682
Tang, J., Sun, L., & Yang, S. 2013, Computer Applications and Software, 7, 037
Wu, F., Liu, J., Ren, X., & et al. 2013, Acta Optica Sinica, 33, *http://www.cnki.com.cn/Article/CJFDTotal-GXXB201311023.htm*